Citation for published version:
Misra, M, Andrews, SR & Maier, SA 2012, 'Waveguide artefacts in terahertz near field imaging', *Applied Physics Letters*, vol. 100, no. 19, 191109. https://doi.org/10.1063/1.4714532

DOI:
10.1063/1.4714532

Publication date:
2012

Document Version
Publisher's PDF, also known as Version of record

Link to publication

Copyright 2012 American Institute of Physics. This article may be downloaded for personal use only. Any other use requires prior permission of the author and the American Institute of Physics.
The following article appeared in Misra, M., Andrews, S. R. and Maier, S. A., 2012. Waveguide artefacts in terahertz near field imaging. Applied Physics Letters, 100 (19), p. 191109 and may be found at http://dx.doi.org/10.1063/1.4714532

University of Bath

Alternative formats
If you require this document in an alternative format, please contact:
openaccess@bath.ac.uk

General rights
Copyright and moral rights for the publications made accessible in the public portal are retained by the authors and/or other copyright owners and it is a condition of accessing publications that users recognise and abide by the legal requirements associated with these rights.

Take down policy
If you believe that this document breaches copyright please contact us providing details, and we will remove access to the work immediately and investigate your claim.

Download date: 05. May. 2023

Waveguide artefacts in terahertz near field imaging

M. Misra,[1,a)] S. R. Andrews,[1,b)] and S. A. Maier[2]
[1]*Department of Physics, University of Bath, Bath BA2 7AY, United Kingdom*
[2]*Department of Physics, Imperial College London, London SW7 2AZ, United Kingdom*

(Received 12 March 2012; accepted 24 April 2012; published online 9 May 2012)

We report experimental and computational studies of the behaviour of a photoconductive THz near field probe when imaging a simple planar metal-dielectric structure. We show that the excitation of waveguide modes in the gap between sample and probe, together with diffraction at the probe, must generally be taken into account when analysing images and that electromagnetic simulations provide a very useful aid to interpretation. © *2012 American Institute of Physics*. [http://dx.doi.org/10.1063/1.4714532]

Developments in the terahertz frequency band are strongly motivated by applications in fundamental science and the quest for new imaging and sensing modalities. Examples of current or emerging applications include the characterization of materials, medical imaging, pharmaceutical quality control, security screening, and biochemical sensing.[1] In many of these applications, a deep sub-mm scale resolution is often desired, which requires the development of near field imaging with scanning probes. An accurate knowledge of the near field is also crucial for the emerging area of designer THz materials based on the spoof surface plasmon polariton concept.[2,3] Approaches to near field microscopy can be broadly divided into techniques which utilize apertures and those which are apertureless. In the former case, a sub-wavelength active area of a source or detector is defined by means of a static[4,5] or dynamic[6] aperture or by the focal spot size of a pump or probe laser beam when using a nonlinear optical crystal for difference frequency generation or electro-optic detection of THz radiation.[7] In the apertureless method, radiation is typically scattered by the end of a sharp metal probe tip and collected in the far[8] or near field.[9] Near field THz techniques have been employed to study a variety of metal-dielectric structures such as sub-wavelength apertures,[7] metamaterials,[10] semiconductor devices,[11] and waveguides.[12] As with other scanning probe microscopies, there is a need to understand the probe-sample interaction in order to correctly interpret images and perform quantitative measurements. This is potentially very important for metallic probes that can significantly change local fields. In this letter, we describe THz time domain experiments and complementary numerical simulations designed to study the interaction between a photoconductive near field probe with integrated metal aperture and a simple planar metal-dielectric test structure.

The test structure, shown in Fig. 1, consists of a 300 nm thick large area, rectangular Ti/Au film deposited on the front of a 500 μm thick, high resistivity silicon substrate and illuminated from the back by a broad THz beam from a conventional single-cycle-like GaAs photoconductive source. The imaging coordinate system is referenced to an edge of the gold film, which is located at the centre of the sample as shown in Fig. 1. The probe was scanned in a direction perpendicular to the gold edge (i.e., along x) at a constant z separation from the gold surface of typically 20 μm.

The probe receiver design is similar to that described by Mitrofanov *et al.*[4] It is based on a 10 μm long, Ti/Au dipole receiving antenna deposited on a 1 μm thick low temperature (LT) GaAs film and glued antenna face down to a sapphire substrate. The opposite side of the GaAs is coated with a 300 nm thick, 2 mm square aluminium screen with an intervening 1 μm thick SiO_2 electrical isolation layer. The screen has a 20 μm square aperture, centred over the dipole antenna. The sample is stationary and the probe is positioned by motorized translation stages with backside optical gating pulses delivered by hollow core photonic crystal fibre. Parallel alignment of the sample and probe front surfaces is accomplished by small adjustments of the sample tilt at large sample-probe separations so as to achieve constant delay between the main pulse and the THz echo arising from reflection of the THz beam between the two surfaces for ± 0.5 mm probe translation along x or y. Recording echoes at a series of sample-probe separations allows the z position of the probe to be calibrated and maintained constant to an accuracy of ± 1 μm.

Intensity maps showing the variation of receiver current with time delay as the probe is scanned along x are shown in Fig. 2 for polarization parallel ($E//y$, Fig. 2(a)) and

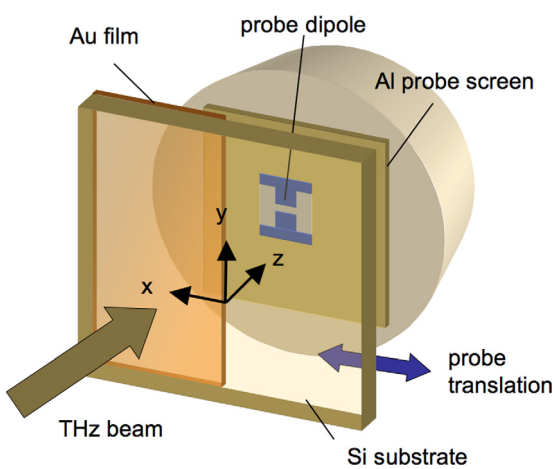

FIG. 1. Schematic of experimental geometry with probe behind the silicon substrate (shown transparent) of the test structure.

[a)]Present address: Department of Physics, University of Warwick, Coventry CV4 7AL, United Kingdom.
[b)]Electronic mail: s.r.andrews@bath.ac.uk.

 © 2012 American Institute of Physics

Downloaded 22 Aug 2012 to 138.38.54.59. Redistribution subject to AIP license or copyright; see http://apl.aip.org/about/rights_and_permissions

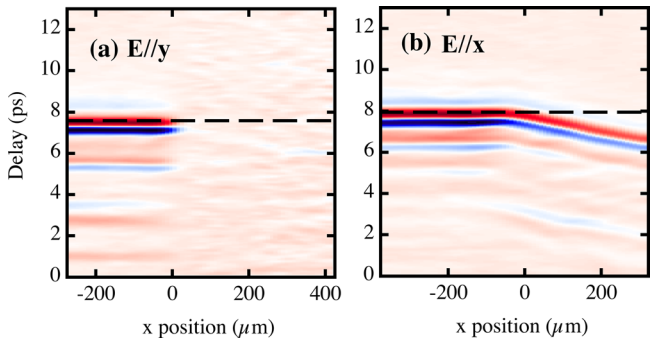

FIG. 2. Intensity maps showing time dependence of receiver current versus probe position along x for THz polarisation (a) parallel to edge (i.e., along y) and (b) perpendicular to edge (i.e., along x). Red indicates positive field, blue negative, and white zero. The sample-probe separation is 20 μm. The dashed lines show the chosen delay, for the amplitude versus x plots in Figs. 3(a) and 3(b).

perpendicular ($E//x$, Fig. 2(b)) to the edge of the gold film. The receiver current is proportional to the x component of the electric field at the probe aperture to a good approximation. For each incident polarization, the probe is rotated about its surface normal so that the dipole axis is oriented for maximum signal. The amplitude at fixed delay is seen to drop off sharply as the probe is moved behind the gold film (positive x) if the polarization of the THz beam is parallel to the edge of the film ($E//y$). For the orthogonal polarization ($E//x$), the fall off is significantly slower. In the latter case, the angled portion of the amplitude-position plot in Fig. 2(b) demonstrates the existence of a wave originating at the gold edge and propagating in the gap between the metal surfaces of the probe and sample. The fall off of the signal amplitude as the probe is scanned across the edge of the gold film at a fixed delay corresponding to the peak signal is shown in more detail for the two incident polarizations in Figs. 3(a) and 3(b). For $E//y$ (Fig. 3(a)), the amplitude decreases over a length scale very similar to the sum of aperture size and sample-probe separation as the probe traverses behind the

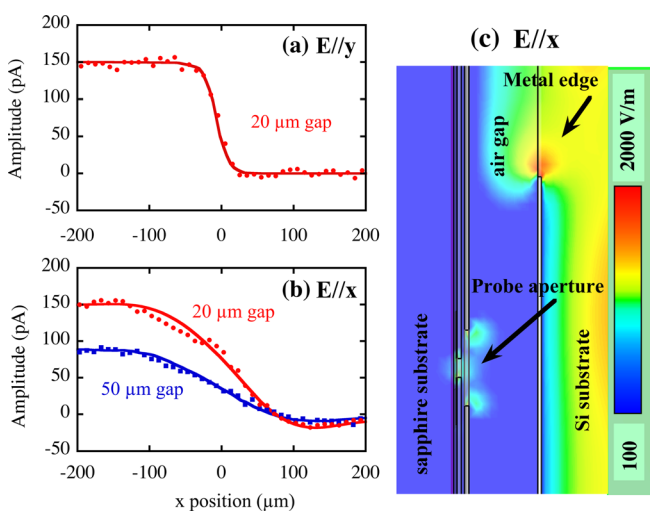

FIG. 3. (a) Measured (points) and calculated (solid curve) peak receiver current at fixed delay for the sample-probe gaps indicated. (a) Results for THz polarisation parallel to the gold edge and (b) for perpendicular polarisation. (c) Logarithmic time average E_x map in the $y = 0$ plane for incident polarization perpendicular to the gold edge. The centre of the probe aperture is located at $x = 50$ μm, $z = 20$ μm.

gold film, as expected. The slower decrease for $E//x$ shown in Fig. 3(b) was noted, but not explained, more than ten years ago.[4,5] Similar behaviour at metal edges has recently been attributed to the excitation and propagation of surface plasmon polaritons (SPPs).[13] However, by closely comparing experiment with finite element simulations described below, we find that the behaviour in the present case can be quantitatively accounted for by the excitation of a TEM-like waveguide mode in the air gap between probe and sample together with a cross polarization probe sensitivity associated with scattering at the aperture. Although there must be finite coupling to the conduction electrons in the gold and aluminium films so that strictly speaking the mode should be regarded as a combination of SPPs bound to the two metal surfaces, we find that the difference between such a mode and the TEM mode of a perfectly conducting parallel plate guide, which does not support SPPs, is very small in a typical near field measurement geometry, consistent with the small fraction of the field in metal at THz frequencies.

Time domain electromagnetic simulations were performed using the finite integration technique[14] with the sample illuminated by a 3 THz bandwidth plane wave. The front metallised areas of the probe and sample were first treated in the perfect electric conductor (PEC) approximation and then, for comparison, in a more realistic Drude model, taking values for the plasma frequency and scattering time of gold and aluminium from Ref. 15. Both approaches gave very similar results for the magnitude and spatial variation of the fields and receiver current, as discussed further below. The conductivity of the LT GaAs photoswitch bridging the 5 μm gap between the arms of the dipole antenna was maintained constant at its "on" value rather than simulating the sampling mode of operation of the real probe. The dielectric function of the LT GaAs was treated in a Drude model with a plasma angular frequency of 2.4×10^{14} rad/s and scattering time of 55 fs. The carrier density is estimated from the 8 mW average optical gating power and the scattering time from the LT GaAs mobility of 3000 cm^2/Vs which was measured in visible pump-THz probe experiments on the same material. The gold arms of the dipole antenna are also treated in a Drude approximation. The THz field that reaches the antenna generates a current in the arms and it is this quantity that is compared with the measured receiver current. The calculated results for the peak receiver current at fixed delay in the PEC case are shown by the curves in Figs. 3(a) and 3(b). In these simulations, the probe was stepped along the x-axis. There is close agreement with experiment using only a single amplitude scaling factor. The reason for the different behaviour for $E//x$ and $E//y$ can be understood with the aid of the field map in Fig. 3(c) which shows the calculated time average of E_x for incident polarization perpendicular to the gold edge ($E//x$). It is apparent that E_x falls off quickly in the shadow of the gold film, in a very similar manner to that for $E//y$, but grows again in the region of the aperture. Diffraction at the gold edge very efficiently couples the x-polarised incident wave into the z polarized TEM (TM_0) mode of the parallel plate waveguide formed between the metallic sample and probe surfaces. Such coupling does not occur for the orthogonal incident polarization. The TEM mode has no cut-off and no z variation of electric field within the waveguide. For

Downloaded 22 Aug 2012 to 138.38.54.59. Redistribution subject to AIP license or copyright; see http://apl.aip.org/about/rights_and_permissions

sample-probe separations of 50 μm or less, higher order TM modes are cut off within the 3 THz system bandwidth. The dipole and aperture together diffract part of the TEM mode to generate an additional x field component at the antenna proportional to the difference in E_z across the aperture.[16] The measured signal is thus proportional to $E_x + adE_z/dx$, where a is a constant proportional to the aperture size. Experimentally and computationally, we find that similar guiding and cross polarization effects also occur for an apertureless photoconductive probe which is identical to the probe previously described except for the absence of the aluminium screen. In this case, guiding takes place between metal and dielectric surfaces and the dipole antenna alone acts as the scatterer.

Fig. 4(a) shows the calculated variation of the peak to peak amplitudes of the x and z field components 10 μm in front of the sample in the case that the probe aperture is closed by metal (solid curves) and in the case that the probe is completely removed from the simulation (dashed curves). Calculations are in the PEC approximation for incident polarization along x. The field component E_x, which is perpendicular to the test edge, decays behind the gold film in an identical fashion to the case in which the incident polarization is parallel to the edge. By comparison with the case that the probe is removed, it can be seen that the main perturbing effects of the probe are a spatially uniform screening of E_x and the generation of a much larger z field component with a different spatial variation. The points in Fig. 4(a) show the results of calculations using a Drude conductivity model in which SPPs are supported. The extremely close similarity between the PEC and Drude calculations in Fig. 4(a) provides the basis for our previous assertion that the guided wave has very weak SPP character.

A further check on the ability of the calculations to describe experiment is provided by comparing predicted and measured results for the peak to peak field versus x. Fig. 4(b) shows there is again excellent agreement with only a single amplitude scaling factor. Opening an aperture in the metal sheet further changes E_z. In particular, it leads to a shift in the maximum gradient of E_z, which gives the maximum signal for $E//x$ in Fig. 4(b), to more negative x. The fall off in peak to peak signal for $E//x$ as the probe moves further into the shadow of the gold film is explained by the decrease of dE_z/dx as the wave in the gap between probe and sample evolves from the incident plane wave into the TEM-like guided mode for which E_z is independent of x in the absence of attenuation.

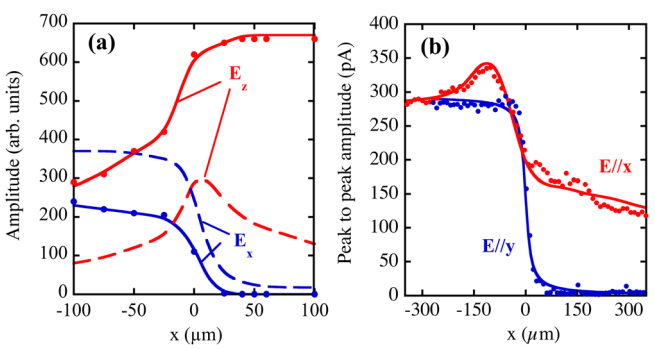

FIG. 4. (a) Solid curves show calculated x variation of peak to peak electric field amplitudes E_z and E_x in the middle of the sample-probe air gap ($z = 10$ μm) for sample-probe separation of 20 μm, incident polarization $E//x$, and probe aperture closed with metal. Dashed curves show fields with no probe. All curves show calculations in the PEC approximation and points show results obtained using a Drude conductivity model. (b) Measured (points) and calculated (solid curves) amplitude of the receiver signal for incident THz polarizations shown. Probe is stepped along the x-axis with a probe-sample separation of 20 μm.

In conclusion, we have experimentally studied the near field of a planar metal-dielectric test object illuminated by a THz beam using an aperture type photoconductive probe. With the aid of electromagnetic simulations, we find that that in general the probe has more than just a uniform screening effect on the measured field because of a polarization dependent coupling into waveguide modes in the gap between probe and sample and a cross polarization detection effect associated with coherent scattering at the probe dipole and aperture. Similar behaviour is found for planar photoconductive probes both with and without apertures, thus placing some fundamental constraints on the ability of any planar probe to quantitatively study planar structures, although we note that numerical simulations are very effective in predicting behaviour if the structure is known. We also find that intrinsic surface plasmon polaritons have no discernable affect on the field distribution on the sub-mm length scales typically involved in THz near field microscopy, which considerably simplifies modeling and contrasts with their clear involvement on cm length scales at terahertz frequencies[17] and their important role in near field microscopy at optical frequencies.[18]

We thank the Royal Society and the Airforce Office of Scientific Research for financial support.

[1]X.-C. Zhang and J. Xu, *Introduction to Terahertz Wave Photonics* (Springer, New York, 2010).
[2]C. R. Williams, M. Misra, S. R. Andrews, S. A. Maier, S. Carretero-Palacios, S. G. Rodrigo, F. J. García-Vidal, and L. Martín-Moreno, Appl. Phys. Lett. **96**, 011101 (2010).
[3]A. I. Fernández-Domínguez, C. R. Williams, F. J. García-Vidal, L. Martín-Moreno, S. R. Andrews, and S. A. Maier, Appl. Phys. Lett. **93**, 141109 (2008).
[4]O. Mitrofanov, I. Brener, R. Harel, J. D. Wynn, L. N. Pfeiffer, and K. W. West, Appl. Phys. Lett. **77**, 3496 (2000).
[5]S. Hunsche, M. Koch, I. Brener, and M. C. Nuss, Opt. Commun. **150**, 22 (1998).
[6]Q. Chen, Z. Jiang, G. X. Xu, and X.-C. Zhang, Opt. Lett. **25**, 1122 (2000).
[7]A. J. L. Adam, J. M. Brok, M. A. Seo, K. J. Ahn, D. S. Kim, J. H. Kang, Q. H. Park, M. Nagel, and P. C. M. Planken, Opt. Express **16**, 7407 (2008).
[8]H.-T. Chen, R. Kersting, and G. C. Cho, Appl. Phys. Lett. **83**, 3009 (2003).
[9]N. C. J. van der Valk and P. C. M. Planken, Appl. Phys. Lett. **81**, 1558 (2002).
[10]A. Bitzer, H. Merbold, A. Thoman, T. Feurer, H. Helm, and M. Walther, Opt. Express **17**, 3826 (2009).
[11]A. J. Huber, F. Keilman, J. Wittborn, J. Aizpurua, and R. Hillenbrand, Nano Lett. **8**, 3766 (2008).
[12]O. Mitrofanov, T. Tan, P. R. Mark, B. Bowden, and J. A. Harrington, Appl. Phys. Lett. **94**, 171104 (2009).
[13]R. Mueckstein, C. Graham, C. C. Renaud, A. J. Seeds, and J. A. Harrington, J. Infrared Millim. Terahz Waves **32**, 1031 (2011).
[14]CST MICROWAVE STUDIO, Computer Simulation Technology GmbH, Darmstadt, Germany.
[15]M. A. Ordal, R. J. Bell, R. W. Alexander L. L. Long, and M. R. Querry, Appl. Opt. **24**, 4493 (1985).
[16]R. Muckenstein and O. Mitrofanov, Opt. Express **19**, 3212 (2011).
[17]J. Liu, R. Mendis, and D. M. Mittleman, Appl. Phys. Lett. **98**, 231113 (2011).
[18]*Near Field Optics and Surface Plasmon Polaritons*, Topics in Applied Physics Vol. 81, edited by S. Kawata, M. Ohtsu, and M. Irie (Springer, Berlin, 2001).

Downloaded 22 Aug 2012 to 138.38.54.59. Redistribution subject to AIP license or copyright; see http://apl.aip.org/about/rights_and_permissions